Journal of Robotics and Control (JRC)
Volume 5, Issue 5, 2024
ISSN: 2715-5072, DOI: 10.18196/jrc.v5i5.22895

Soft Tissue Compliance Detection in Minimally Invasive Surgery: Dynamic Measurement with Piezoelectric Sensor Based on Vibration Absorber Concept

Radwa Hashem [1*], Haitham El-Hussieny [2], Shinjiro Umezu [3], Ahmed M. R. Fath El-Bab [4]
[1, 2, 4] Department of Mechatronics and Robotics Engineering, Egypt-Japan University of Science and Technology (E-JUST), Alexandria 21934, Egypt
[3] Department of Modern Mechanical Engineering, Waseda University, 3-4-1 Okubo, Shinjuku-ku, Tokyo 169-8555, Japan
Email: [1] radwa.hashem@ejust.edu.eg, [2] haitham.elhussieny@ejust.edu.eg, [3] umeshin@waseda.jp,
[4] ahmed.rashad@ejust.edu.eg
*Corresponding Author

***Abstract*—Recent research in the medical field has increasingly focused on tissue repair, tumor detection, and associated therapeutic techniques. A significant challenge in Minimally Invasive Surgery (MIS) is the loss of direct tactile sensation by surgeons, as they cannot physically feel the organs they operate on. Tactile feedback enhances patient safety by tissue differentiation and reducing inadvertent damage risks. Addressing this challenge, this study introduces a novel tactile sensor designed for compliance detection to enhance tactile feedback in MIS. The sensor operates on a 2-Degree-of-Freedom (2-DOF) vibration absorber system, utilizing a piezoelectric actuator with a calibrated stiffness of 188 N/m. It interprets tissue stiffness regarding a spring constant, Ko, and measures changes in soft tissue stiffness by analyzing variations in the vibration absorber frequency, specifically at the frequency which causes the first mass to exhibit zero amplitude. The effectiveness of this sensor was evaluated through tests on polydimethylsiloxane (PDMS) specimens, which were engineered to replicate varying stiffness found in human organ tissues. Young's modulus of these specimens was determined using a universal testing machine, showing a range from 10.12 to 226.89 kPa. Additionally, the sensor was applied to measure the stiffness of various chicken tissues – liver, heart, breast, and gizzard with respective Young's moduli being 1.97, 9.47, 19.55, and 96.36 kPa. This sensor successfully differentiated between tissue types non-invasively, without requiring substantial deformation or penetration of the tissues. Given its piezoelectric nature, the sensor also holds significant potential for miniaturization through Micro-Electro-Mechanical Systems technology (MEMS), broadening its applicability in surgical environments.**

Keywords—Tactile Sensor; Soft Tissue; Compliance Detection; Vibration Absorber; MIS; Piezoelectric Actuator.

I. INTRODUCTION

Historically, surgical procedures predominantly involved conventional open surgery, necessitating large incisions. The advent of Minimally Invasive Surgery (MIS) marked a significant shift in this paradigm. MIS, now widely practiced across various medical specialties, utilizes significantly smaller incisions, offering numerous benefits such as reduced pain, faster recovery, lower infection risk, minimal scarring, and decreased bleeding [1]-[7]. Despite these advantages, MIS poses a challenge regarding the loss of tactile feedback, which is inherently present in open surgery. This tactile information is crucial, as it aids surgeons in making informed decisions during operations.

Artificial tactile sensing technologies have emerged as a solution to mitigate this loss of tactile perception in MIS. These technologies enable the recovery of critical tactile information without inflicting harm, discomfort, or tissue damage to the patient. This is particularly beneficial for clinicians who rely heavily on their sense of touch during physical examinations and palpation, a routine practice in traditional diagnostics and surgeries [8]-[13]. Artificial tactile sensors play a pivotal role in these scenarios, offering an objective means to measure tissue compliance. This feature is invaluable in tasks such as detecting cancerous lumps or assessing tissue health, which traditionally relied on significant incisions [14]-[17].

The integration of Micro Electromechanical Systems (MEMS) in MIS has seen a rapid expansion due to these emerging needs and applications. Extensive research has been conducted to ascertain the mechanical properties of soft tissues surrounding internal organs [18]-[26]. Moreover, tactile sensing has found applications beyond the medical field, including stiffness detection in various domains [27]-[31]. Significantly, cancerous tissues often exhibit greater stiffness compared to healthy tissues [32]-[39], enabling clinicians to assess conditions such as liver [40] and breast tumors [41] based on tissue compliance. In MIS, compliance detection during soft tissue palpation tasks is crucial for identifying cancerous tissues [42]-[48]. Mechanical models typically represent soft tissues as having a flat substrate, from which Young's modulus can be derived through indentation tests [49]-[52]. The concurrent measurement of indentation force and depth is instrumental in evaluating the stiffness of the targeted soft tissue [53]-[55]. This approach underscores the growing importance and utility of tactile sensing and MEMS technology in enhancing the efficacy and safety of MIS procedures.

The impact of diseases on the mechanical properties of various human tissues has been a subject of extensive research, leading to significant findings. For example, liver disease results in a marked increase in tissue stiffness, with diseased liver samples exhibiting an elastic modulus approximately three times higher than that of healthy liver tissue. In vivo investigations using a small indenter revealed that sick human liver samples possessed an average elastic modulus of 0.74 MPa, significantly stiffer than the 0.27 MPa typically observed in healthy liver tissue [56].

Similarly, notable variations in the elastic modulus have been documented in other human tissues. Indentation testing has shown that the brain's elastic modulus ranges between 0.5 and 1 kPa [57], with its Young's modulus reported to be between 0.3 and 10 kPa [58]. In the case of cartilage, the elastic modulus is considerably higher, ranging from 450 to 800 kPa [59]. Additionally, the elastic modulus of kidney tissue varies across different regions, with values estimated at 24.5 kPa and 62.3 kPa based on the interaction forces between a probe and the kidney's surface [60].

Further expanding the scope of research in this area, a study [61] developed a system using a robotic device equipped with a force transducer to measure the mechanical properties of live pig tissues. This system successfully determined the stiffness and Young's modulus of liver tissue, which were found to be 127 N/m and 31.8 kPa, respectively. In the lower esophagus tissue, stiffness measurements reached 195 N/m, with Young's modulus of 48.8 kPa. These studies collectively underscore the significance of understanding tissue mechanics, not only for diagnostic purposes but also for the development of more effective surgical tools and techniques in treating various diseases.

Tactile sensors, which are integral to MIS, can be broadly classified based on their sensing mechanisms [62]. From a transactional viewpoint, these sensors are typically categorized as capacitive [63]-[65], resistive [66]-[70] or piezoelectric [71]-[77]. In the current market, most tactile sensors are designed either for static or dynamic applications. Static or passive tactile sensors operate on the fundamental principle that tissue deformation under applied force correlates with its stiffness [78]-[81]. These sensors are crucial in applications where steady pressure is applied and the resultant deformation is measured to assess tissue characteristics [82]-[86].

As highlighted in sources [87], [88], among the various types of tactile sensors, cantilever-based sensors employing piezoelectric elements are particularly effective and widely used. These sensors leverage the piezoelectric effect to both sense and actuate signals. One of the key advantages of piezoelectric sensors is their capability for self-sensing and actuation [89]-[93]. This means that they can generate an electrical signal in response to applied mechanical stress, and conversely, they can produce mechanical motion when an electrical field is applied.

Furthermore, the compatibility of piezoelectric sensors with MEMS technology is a significant benefit. MEMS technology enables the miniaturization of these sensors, making them highly suitable for MIS applications where space constraints are a critical factor. The integration of piezoelectric sensors with MEMS technology allows for the development of more compact, efficient, and sensitive tactile sensors. This combination enhances the surgeon's ability to assess and interact with tissues, contributing significantly to the precision and safety of minimally invasive surgical procedures.

To enhance tissue stiffness assessment in Minimally Invasive Surgery (MIS), a tactile sensor leveraging piezoelectric technology has been developed. This sensor operates by detecting variations in resonant frequency upon contact with tissue, thereby determining tissue stiffness [94]. Utilizing a piezoelectric bimorph, the sensor is capable of distinguishing between similar soft materials, which is particularly crucial in procedures like precise brain tumor removal. Its operation involves a random phase multi-sine input, and it evaluates contact properties through the Frequency Response Function (FRF) [95].

Furthermore, a resonant tactile sensor specifically designed for MIS applications has been introduced to detect tissue stiffness by measuring changes in resonant frequency during interaction with different tissues [96], [97]. Incorporating a PZT (lead zirconate titanate) bimorph that functions as both an actuator and a sensor, this design is notably streamlined. The sensor identifies shifts in resonant frequency by monitoring alterations in the electrical impedance during resonance, providing a simple yet effective means to evaluate tissue stiffness [98].

In this study, we developed a tactile sensor specifically designed for the detection of soft tissue stiffness. This sensor is based on a 2-degree-of-freedom (2-DOF) vibration absorber model, which is particularly chosen to mitigate the risk of damage that might arise from resonance effects. The parameters of the sensor were meticulously identified and optimized using MATLAB software, ensuring precise and reliable performance.

To validate the sensor's applicability, we conducted experimental measurements using a variety of polydimethylsiloxane (PDMS) samples and soft tissues. These experiments included indentation tests, which are pivotal for assessing the mechanical properties of soft tissues. The results from these tests have demonstrated the piezoelectric sensor's effectiveness in accurately detecting tissue stiffness. This efficiency not only validates the sensor's design but also underscores its potential for enhancing diagnostic capabilities in medical applications, particularly in the context of minimally invasive surgery.

II. SENSOR MODEL

The measurement system implemented in the study is designed as a 2-degree-of-freedom (2-DOF) system, as illustrated in Fig. 1. This system is constituted by two masses, denoted as m_1 and m_2, and two springs, labeled K_1 and K_2. The primary function of this configuration is to accurately measure the stiffness of soft tissue, represented as K_o.

The mathematical model underpinning this system is derived following the methodology outlined in [99]. This process involves a detailed analysis of the dynamics of the 2-DOF system, considering the interaction between the masses and springs and their impact on measuring tissue stiffness.

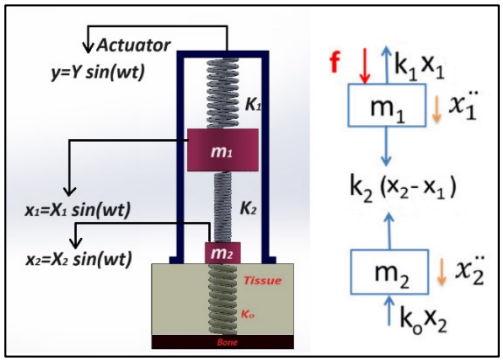

Fig. 1. Two degrees of freedom system

A. System Description

As mentioned in the previous section, the sensor is modeled with two masses and two springs, where m_1 is a large mass, m_2 is a small mass, K_1 is a large spring stiffness, and K_2 is a small stiffness. The stiffness of the soft tissue will be expressed as K_o as shown in Fig. 1. The system is subjected to a sinusoidal input force affecting the main mass m_1 and equals $F = F_o \sin(\omega t)$, where F_o is the amplitude of the input force and $(\omega/2\pi)$ is the frequency. The system is intended to exhibit the vibration absorber phenomenon, where it can effectively absorb or reduce the vibrations generated by the input force, and the system is designed to satisfy the vibration absorber phenomena as in [99], [100].

When there is no contact between the system and the object (at K_o equals zero), the system can achieve vibration absorption when operating at a specific frequency ($\omega = \omega_{22} = \omega_{11}$). This is achieved when the displacement of mass m_1 is zero and all excitation energy is absorbed by mass m_2. The absorber part (m_2, K_2) counteracts the applied force on m_1 with an equal and opposite force [99], [100]. Thus, if the sensor meets an object with different stiffness, the natural frequencies of the overall system are altered, including the vibration absorber frequency (ω_{abs}). Assuming the natural frequencies of the two springs as:

$$\omega_{11} = \sqrt{\frac{K_1}{m_1}} \text{ and } \omega_{22} = \sqrt{\frac{K_2}{m_2}} \tag{1}$$

The amplitude of the displacement of the two masses due to the applied force are X_1, X_2, respectively.

$$X_1 = \frac{[\frac{f}{K_2}]\,[(1+\frac{K_o}{K_2}) - (\frac{\omega}{\omega_{22}})^2]}{[(1+\frac{K_2}{K_1}) - (\frac{\omega}{\omega_{11}})^2][(1+\frac{K_o}{K_2}) - (\frac{\omega}{\omega_{22}})^2] - \frac{K_2}{K_1}} \tag{2}$$

$$X_2 = \frac{X_1}{(1+\frac{K_o}{K_2}) - (\frac{\omega}{\omega_{22}})^2} \tag{3}$$

Defining the amplitudes ratio R as

$$R = \frac{X_1}{X_2} = 1 - \frac{m_2\omega^2}{K_2} + \frac{K_o}{K_2} \tag{4}$$

As depicted, R is a function of (ω, K_o, K_2, m_2) and it is not dependent on K_1, and m_1.

To study the effects of each parameter (ω, K_o, K_2, m_2) on the amplitude ratio (R), apply partial derivatives for (4):

$$\frac{\partial R}{\partial \omega} = -\frac{(2\, m_2 \omega)}{K_2}, \ldots . non\ linear \tag{5}$$

$$\frac{\partial R}{\partial\, m_2} = -\frac{\omega^2}{K_2}, \ldots .\ linear\ at\ certain\ \omega,\ K_2 \tag{6}$$

$$\frac{\partial R}{\partial\, K_o} = \frac{1}{K_2}, \ldots .\ linear\ at\ certain\ K_2 \tag{7}$$

$$\frac{\partial R}{\partial\, K_2} = \frac{m_2\omega^2 - K_o}{K_2^2}, \ldots .\ not\ linear \tag{8}$$

Let: m_2 and K_2 be selected to make $\omega_{22} = \omega$ which refers to achieving no resonance to get linear relationship.

$$K_o = R\, K_2 \tag{9}$$

The sensor measures the stiffness changes (K_o) by measuring the shock absorber's frequency (ω_{abs}). When the sensor interacts with an object of varying stiffness, causing a vibration absorber frequency shift (ω_{abs}) as shown in (13), this relationship enables the sensor to determine the object stiffness. The vibration absorption phenomena occur at $X_1 = 0$.

$$\left[\left(1+\frac{K_o}{K_2}\right) - \left(\frac{\omega}{\omega_{22}}\right)^2\right] = 0 \tag{10}$$

$$X_2 = \frac{f}{K_2} \tag{11}$$

$$\omega_{abs} = \sqrt{{\omega_{22}}^2(1+\frac{K_o}{K_2})} \tag{12}$$

$$K_o = K_2\,(\frac{{\omega_{abs}}^2}{{\omega_{22}}^2} - 1\,) \tag{13}$$

B. The Soft Tissue Model and Measuring Range

In this section the soft tissue is modeled as a cube with height (h). If the soft tissue is excited by vertical load F acting over an indentor of radius, r as shown in Fig. 2, then the stiffness can be expressed according to Hayes model [101] and the soft tissue stiffness can be expressed as the following equation:

$$K_o = \frac{2rEC_k}{(1-\nu^2)} \tag{14}$$

Where K_o is tissue stiffness and it equals F/d. F is the applied force needed to produce displacement, h is the tissue height from a bone layer, d is the indentation depth, r is the radius

of the indentor, ν, and E are Poisson's ratio and Young's modulus of the tissue moreover, C_k is a scaling factor (geometry dependent factor) depends on ν, aspect ratio (r/h) and deformation ratio (d/h) [101].

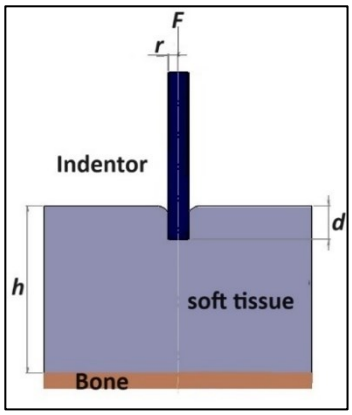

Fig. 2. Indentation model parameters

For determining the measuring range of the sensor, some literatures show the following**:** According to [56] normal liver has a Young's modulus of 270 kPa and a defective liver has a Young's modulus of 740 kPa. Thus, Young's modulus for the present study will be assumed to be 1 MPa and Poisson's ratio equals 0.5 based on previous studies for soft tissue. Assumed par0ameters for the plane-ended cylindrical indentor to get stability in readings as proved in [102]. The parameters are, h = 5 mm, tissue height, r = 1 mm, indentor radius, from table (3) in [103] at r/h = 0.2, ν = 0.5, and d/h=0.1% C_k equals 1.244 and C_k= 1.356 at d/h=10% for maximum deformation considering the friction between indentor and the skin. Taking the mean value of C_k = 1.300, E = 1 MPa, ν = 0.5, and r = 1 mm for the calculation of K_o using (14), K_o equals 3.46 N/mm. Finally, the tissue stiffness range will be taken from 0 to 4 kN/m to carry out the design. Taking into consideration that the value of the measurement range can be changed according to the application as the measuring range depends on the scaling factor C_k, which changes from 1.244 to 1.356 according to the tissue deformation percentages and the indentor size. Mention that while forcing the sensor against the tissue, the sensor output reading according to different tissue compliance will change.

III. SENSOR PARAMETERS SELECTION

This section describes the guidelines for selecting the sensor parameters, m_1, K_1, m_2, and K_2:

- To ensure compliance with the vibration absorber, it is first necessary to satisfy the ratio between the stiffness of the springs and the masses, so that: $\sqrt{\frac{K_1}{m_1}} = \sqrt{\frac{K_2}{m_2}}$.
- A value of 0.5 for m_2/m_1 is then chosen to facilitate zero displacement at m_1 [99]
- It is recommended that the relationship between ω_{abs}-K_o, remains linear across the working range, to maintain consistency of measurement along the measuring range.
- The selection of vibration absorber parameter, K_2 and m_2 should be chosen to achieve higher accuracy when detecting soft tissue stiffness K_o.
- Finally, it is recommended to keep the masses m_1 and m_2 as small as possible to increase the frequency range at certain values of K_1 and K_2.

The system is intended to measure tissue stiffness change, potentially detecting diseased tissues. The guidelines above mention considerations such as the ratio of masses between (m_1 and m_2), the need for a linear relationship between frequency and soft tissue stiffness (K_o) a desire for high measurement consistency, and the importance of minimizing mass to increase the frequency range hence more measurement range.

IV. MATHEMATICAL MODEL

In this section the frequency responses of X_1 and X_2, the displacements of the lumped masses m_1 and m_2, respectively, are determined. To ensure the vibration absorber phenomena using MATLAB as in Fig. 3, The responses are determined at different values of K_o using MATLAB, based on (2) and (3). Furthermore, the frequency at which the displacement of m_1 equals zero where the vibration absorber phenomenon occurs. The relation between the soft tissue stiffness (K_o) and the frequency was determined according to (12) besides the frequency responses of each mass in (2) and (3) The association between tissue stiffness and the corresponding frequency (ω_{abs}) at which the vibration absorber operates is established based on specific design parameters to assure the vibration absorber phenomenon mathematically. These parameters include m_2 = 6 gm (assumed), K_2 = 188 N/m (using available Piezo actuator as an example, such as PIEZO SYSTEMS: D220-A4-503YB), m_1 = 2 m_2, and K_1=2 K_2, where criteria 1 and 2 are applied. Fig. 3 illustrates the normalized displacements of the two masses as a function of the excitation frequency at various K_o values.

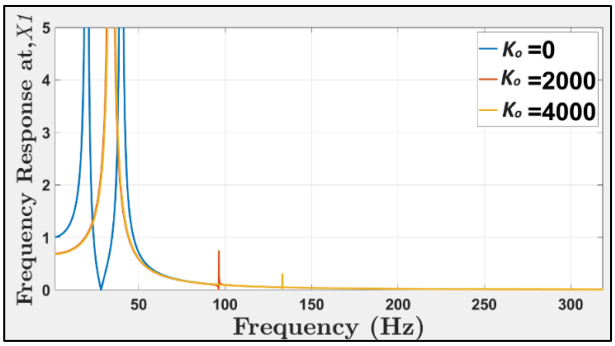

(a)

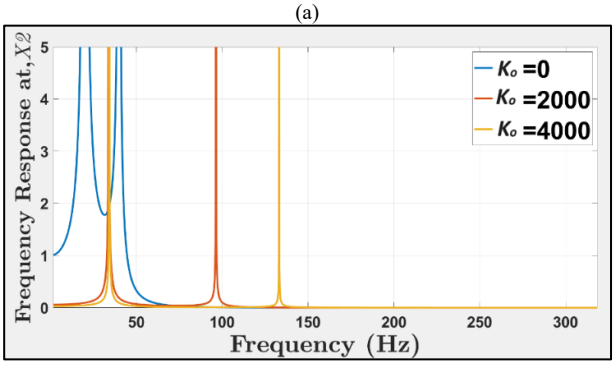

(b)

Fig. 3. Frequency response of (a) X_1 (m_1), and (b) $X_2(m_2)$ at certain tissue stiffness K_o values, and the corresponding vibration absorber frequency ω_{abs}.

V. OPTIMIZING PARAMETERS

The parameter optimization process aims to improve the system functionality and accuracy by identifying the most effective parameter values within constraints and objectives. Fig. 4 shows the schematic diagram for the proposed experimental measurements.

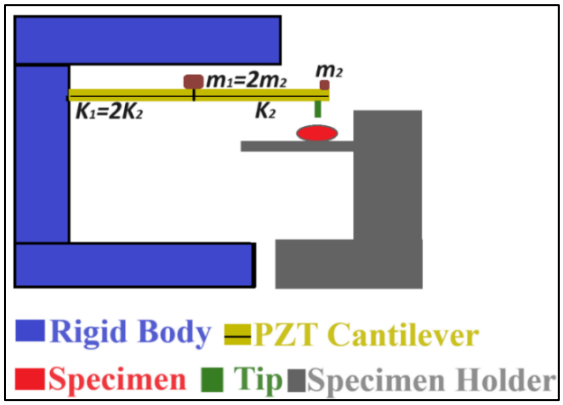

Fig. 4. Schematic diagram for the proposed sensor version

To optimize the system's linearity and measurement range, the parameters of the 2-DOF system were chosen based on available piezoelectric actuators shown in Fig. 5. Through a comparison of measurement range and linearity across various stiffness values, it was evident that higher stiffness not only enhances linearity but also results in a higher measurement range. Each one of them will be tested using MATLAB software to choose which one will achieve the best performance that gives reliability, and best linearity relation between the frequency and the measured stiffness. The concentrated mass of the two actuators is assumed as in [104] by adding the equivalent mass of the beam (0.23 * mass of the piezoelectric beam) at the tip of the cantilever, m_1 and m_2 besides the stiffness as in the datasheet: m_2 = 2.25 gm, K_2= 61 N/m for (D220-A4-103YB) and m_2 4.3 gm, K_2= 188 N/m for (D220-A4-503YB) as mentioned above. Furthermore, m_1= 2 m_2, and K_1= 2 K_2 as mentioned before in section 3 according to [99] to widen the operating range, the masses must be as small as possible.

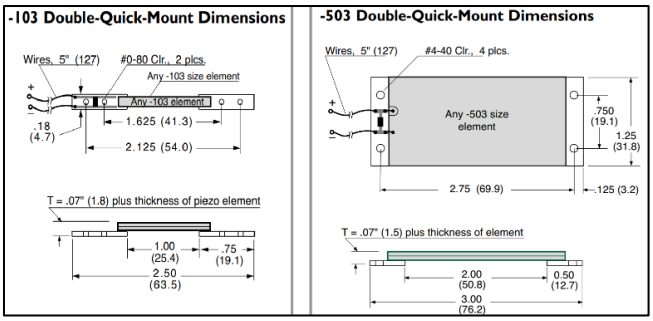

Fig. 5. Piezo actuators systems

To assess the measurement range of the two available piezoelectric actuators and evaluate the system to determine the measurement range of the two piezoelectric actuators, a comprehensive analysis was conducted using MATLAB. Fig. 6 shows cases of the impact of varying tissue stiffness (K_o) on the vibration absorber frequency of the sensor. The MATLAB results present a square correlation (R^2) depicting the linearity between ω_{abs}-K_o within the 0 to 4 kN/m range, using the specified design parameters. It is apparent that the parameters of the first actuator fail to meet the required measurement range. This is primarily attributed to the vibration absorber frequency (ω_{abs}) closely aligning with the second natural frequency of the system within the range of K_o up to 4 kN/m, as illustrated in Fig. 6. a. Consequently, distinguishing the vibration absorber frequency (ω_{abs}) during excitation frequency changes becomes challenging the difference between the second natural frequency and the vibration absorber frequency becomes zero.

Thus, for the first actuator (D220-A4-103YB), the acceptable range falls below 100 N/m, as the difference between the second natural frequency and the vibration absorber frequency is approximately 1 Hz, which is deemed unacceptable. On the other hand, the range of measurements for the second actuator (D220-A4-503YB) extends from 0 to 800 N/m as in Fig. 6. b. The first piezo system (D220-A4-103YB) exhibits lightly lower linearity and a much narrower measurement range. Conversely, the second actuator (D220-A4-503YB) offers superior linearity and a wider measurement range for assessing soft tissue stiffness. Considering the optimization guidelines and our objective of creating a sensor with efficient performance and measurement range, it is evident that the first actuator is unsuitable due to limited measurement range and slightly lower linearity of 95%. Therefore, the best choice would be the second actuator with K_2= 188 N/m.

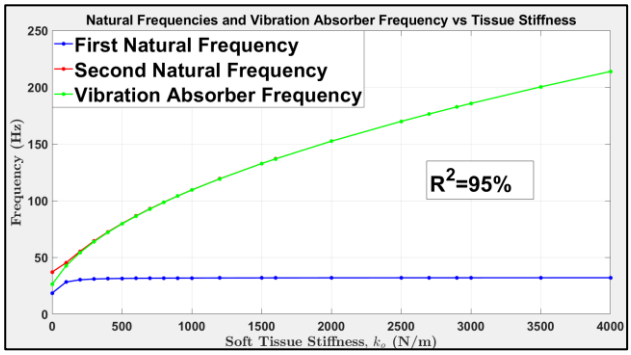

(a) D220-A4-103YB actuator

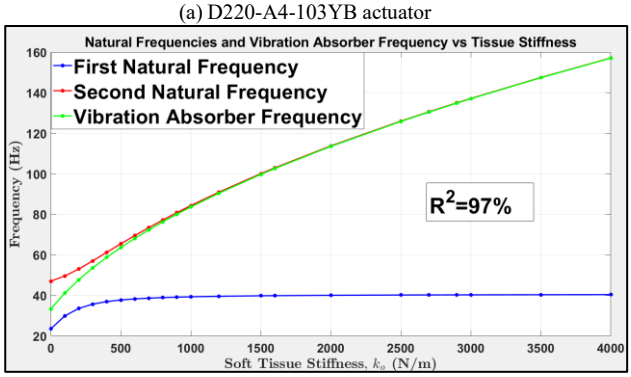

(b) D220-A4-503YB actuator

Fig. 6. Sensor frequencies at different stiffness k_o

VI. DESIGN PROCEDURES OF THE SENSOR

- Commence by determining the appropriate measurement range based on the intended application, as detailed in the above section.

- For addressing the soft tissue scenario, a range of soft tissue properties of Young's modules, 0 to 1 MPa and sensor indentor radius 1 mm to detect a stiffness of (0 to 4 kN/m) is chosen.
- Calculate measurement range and linearity for each value of piezoelectric stiffness based on available types.
- Next, make decisions regarding the masses required at m_1 and m_2, accounting for any additional components (such as bolts). These masses should be minimized to avoid diminishing sensitivity. The system can detect and respond to changes or stimuli. If the masses are too high, it can result in decreased sensitivity, making it harder for the system to detect subtle variations or changes in the measurement.
- The simplified mathematical model presented in (2) and (3) was used to evaluate the performance of the sensor using MATLAB software.
- Leverage a finite element modeling tool to validate the simplified mathematical model and establish the relationship between the vibration absorber frequency ω_{abs} and the tissue stiffness K_o to ensure the vibration absorber phenomena.
- Then, implement the appropriate optimization principles. For instance, consider the optimization criterion of achieving the highest detection range besides a linearity measurement of R^2=97%, as explained in section 5, to identify the optimal combination of a wide range of measurements and linearity to achieve sensitivity during measurement.

VII. EXPERIMENTS

A. FEA Simulation

In this section, the proposed soft tissue compliance sensor is simulated effectively via Finite Element Analysis (FEA) using ANSYS software. Following this, we will thoroughly compare the results with the mathematical model generated in the above section using MATLAB. The CAD model consists of three layers; the 1st layer and the 3rd layer share the same material and thickness, which is PZT-5A, while the middle layer is made of Brass. Table I shows the properties of the material of the Piezoelectric Actuator.

TABLE I. MATERIAL PROPERTIES OF THE PIEZOELECTRIC ACTUATOR

Material Type	Density (kg/m^3)	Modulus of Elasticity (N/m^3)	Poisson's ratio
Brass	8300	1e11	0.32
PZT-5A	7800	5.2e10	0.34

The model consists of the bolts that are used to mount the three actuators together; the mass of each bolt and nut is equal to 0.9 gm besides the acrylic part to support all together at the main mass. Considering that the second mass equals half of the first (main) mass. All parts were scaled, and their weight was reported in grams to be equal to 3.6+1.4 (mass of the bolts and the acrylic part connect the 3 PZT together) at the main mass and 0.7+1.8 (bolts and acrylic part with the tip) at the second mass. The boundary condition in the ANSYS model is fixed support at the end of the first two beams. The mesh settings were optimized in the FEA by selecting the minimum mesh size (1 mm) that provided accurate and reliable results. Here, we simplified the weight of bolts in our CAD model with point masses in FEA analysis. When using ANSYS or similar FEA software, we can assign point masses at the locations where the bolts are in the CAD model. This allows us to account for the weight of the bolts without modeling their detailed geometry, as in Fig. 7.

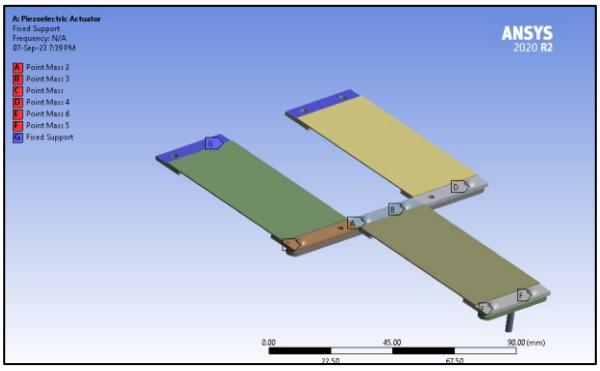

Fig. 7. Boundary conditions applied to the model

Fig. 8 shows the mode shapes of the 1st and 2nd natural frequencies. Furthermore, the mode shape of the system at the vibration absorber frequency which shows the displacement of the main mass near zero at no contact.

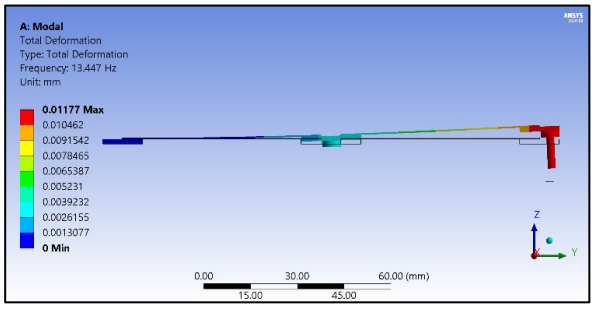

(a)

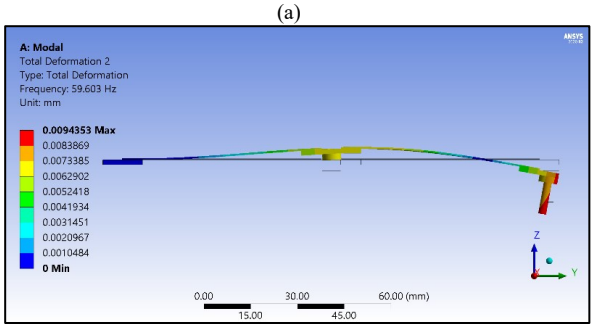

(b)

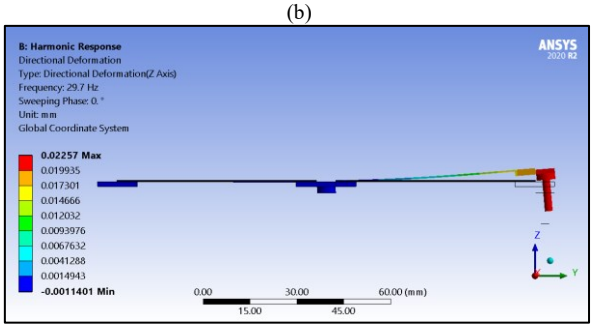

(c)

Fig. 8. The 1st mode shape and (b) 2nd mode shape of the system, and (c) the vibration absorber

The vibration absorber phenomena are achieved at no contact and when it is in contact, as in Fig. 9 and Fig. 10 according to harmonic analysis.

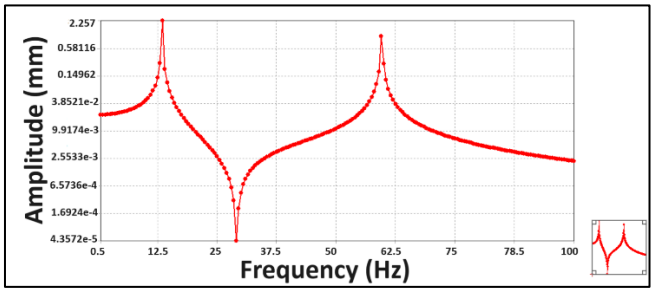

Fig. 9. Frequency response of the system at no contact to the tip of the piezoelectric sensor

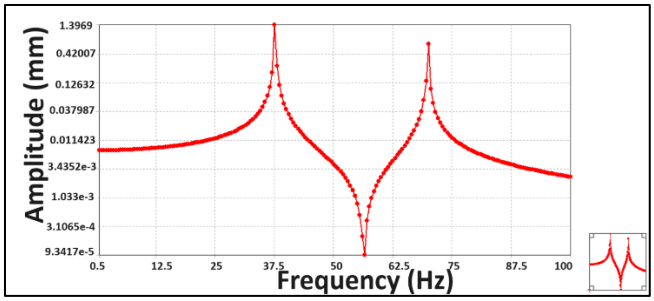

Fig. 10. Frequency response of the system at stiffness 500 n/m attached to the tip

B. *Experimental Work Using D220-A4-503YB Actuator*

In this section, a prototype of the sensor is developed to experimentally confirm the contact sensor's suitability (based on a 2-DOF vibration absorber) for stiffness measurements. The sensor prototype consists of three cantilevers using the Piezoelectric bending actuators D220-A4-503YB. Where the system parameters are K_2=188 N/m, m_2=1.8+0.7= 2.5 gm (bolts+ acrylic part), $K_1 = 2\ K_2$, and $m_1 = 2\ m_2$.

The experimental setup shown in Fig. 11 consists of the piezoelectric sensor, prototype setup of Polymethyl methacrylate (PMMA) was fabricated using VLS3.5 UNIVERSAL LASER SYSTEMS, power supply, function generator, amplifier, eddy current position sensor, and oscilloscope.

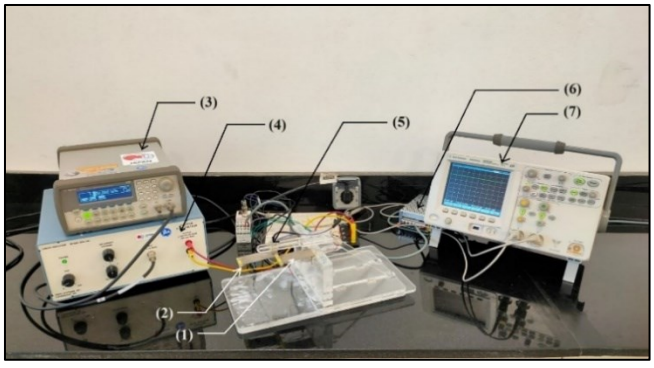

Fig. 11. The experimental setup

(1) Piezoelectric actuator.
(2) Indentor (tip).
(3) Function generator.
(4) Amplifier.
(5) Eddy current sensor.
(6) Power supply.
(7) Oscilloscope.

a) Specimens Preparations:

To assess the effectiveness of the proposed sensor, we prepared four Polydimethylsiloxane (PDMS) specimens shown in Fig. 12 with varying levels of stiffness to replicate the diverse stiffness found in human internal organs tissues [105],[106]. SYLGARD 184 is a popular silicone elastomer kit manufactured by Dow Corning, which is commonly used in various scientific and industrial applications. It consists of two parts: the base elastomer and the curing agent. When these two components are mixed in the correct proportions and cured, they form a flexible and durable silicone rubber material. The mixing ratio between PDMS and the curing agent influences Young's modulus of elasticity (E) for PDMS material. Specifically, Young's modulus decreases as the mixing ratio (elastomer) increases [107]. In other words, when you increase the proportion of curing agent relative to PDMS in the mixture, the resulting PDMS material becomes stiffer and less flexible. This property allows for adjusting the material's elasticity to suit specific applications by controlling the mixing ratio during preparation. The four specimens were mixed at 1:50,1:40,1:30, and 1:20 ratios.

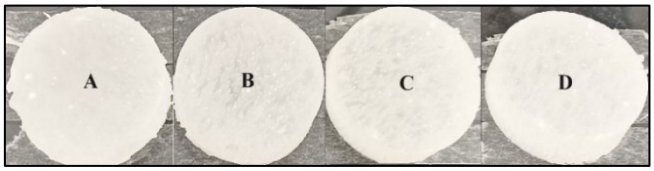

Fig. 12. Four PDMS samples with different stiffness

b) Indentation Test of PDMS:

The indentation approach is used to characterize how a material responds when subjected to applied stress, particularly focusing on its compliant behavior. Indentation is a widely employed method for assessing the mechanical characteristics of softtissues as mentioned in previous studies. A mechanical model is applied to determine Young's modulus of the tissue through an indentation test. Typically, this model assumes that the soft tissue is resting on a flat surface [49]. The Young's modulus of elasticity was determined for the fabricated specimens using Universal Testing Machine (SHIMADZU, J11 0201) shown in Fig. 13 and the indentation test was conducted under low velocity (0.2 mm/min) to avoid damping forces. If the sample is not in complete contact with the indentor and lacks sufficient preload before the indentation test, the elastic modulus of the sample will be underestimated compared to its actual value [108]. As a result, it is necessary to apply preloading to ensure that the test provides precise measurements. After the preloading was applied and the sample was fully contacted, the machine was set to zero and then the test started. The indentor was chosen to be 14 mm and the specimen dimensions were 30 mm in diameter and 10 mm in thickness. The four specimens were fabricated in the same conditions using PMMA mold for 45 minutes and temperature of 100 °C according to the datasheet [109].

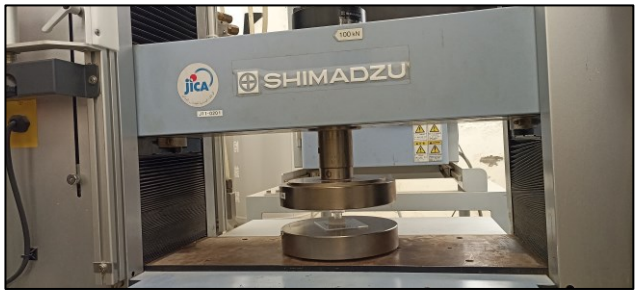

Fig. 13. Universal testing machine (Shimazu, UTM AG X Plus series)

c) Estimation of Young's Modulus for The Specimens:

According to the previous studies [110] Young's modulus was estimated according to [101] [103]. Regarding (14), the final equation of Young's modulus, E will be:

$$E = \frac{F\,(1-\nu^2)}{2rC_k d} \tag{15}$$

Where *F, d, r,* C_k, and ν are applied force, indentation depth, the radius of the indentor, geometry material dependent factor, and Poisson's ratio. The young modulus will be estimated at an aspect ratio (*r/h*) of 0.7 and indentation deformation will be 10% of the original thickness. By taking the mean value of C_k from Table 3 in [103], it will equal 2.818 and Poisson's ratio for PDMS is 0.5 [111].

d) Vibration Analysis of the PDMS Specimens:

Using this experimental setup, we delved into the sensor's response under different conditions: one without any contact (k_o = 0) and another involving contact with materials of varying stiffness. The PDMS specimens mentioned above were used to achieve the target of examining the sensor performance in detecting different stiffnesses. The frequency change of the three frequencies mentioned is observed and the readings were reported.

e) Vibration Analysis of Soft Tissue Specimens:

In this study, our investigation revolved around probing various tissues, the gizzard, breast, heart, and liver samples shown in Fig. 14, using our proposed piezoelectric sensor system. The primary aim is to uncover valuable insights into the mechanical properties of these tissues by analyzing their first, absorber, and second resonant frequencies.

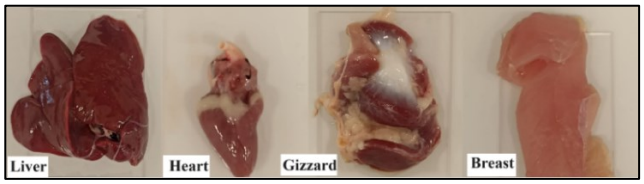

Fig. 14. The specimens used in the test

The use of a piezoelectric sensor system allowed us to apply controlled mechanical stimuli to the tissues and measure their vibration as in Fig. 15. These responses provided critical information about the tissues' elasticity and compliance characteristics, which are essential factors in understanding their biomechanical behavior. Overall, it contributed to a better understanding of the elasticity of the different tissues and showcased the potential of piezoelectric sensors as valuable tools for non-destructive evaluation by introducing the three frequencies.

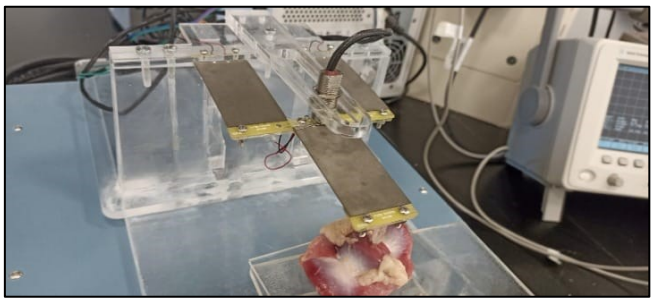

Fig. 15. The experimental testing of the specimen

VIII. RESULTS AND DISCUSSION

The system is established based on the vibration absorber concept to avoid resonance measurements. This concept is checked theoretically using MATLAB software, as in Fig. 3 to ensure that the displacement will equal zero at vibration frequencies. Then it is proven using finite element simulation using ANSYS software and verified experimentally. Optimizing sensor stiffness can significantly enhance sensor performance by extending the frequency range, improving linearity sensitivity, and widening the measurement range, as illustrated in Fig. 6. This optimization process may involve exploring alternative materials, innovative structural designs, or advanced fabrication techniques to achieve optimal stiffness characteristics. Listed below in Fig. 16. a, the results of the finite element model at different stiffness in contact, and Fig. 16. b a comparison between the results of finite elements and mathematical models that achieve the vibration absorber phenomena. The dynamic vibration absorber concept is employed to use the vibration absorber frequency to indicate tumors away from the resonance frequencies. At different values of K_o, it appears that the increase in the stiffness of the third stiffness K_o has led to a change in the behavior of the vibration absorber system and a shift in the system's natural frequencies. This shift could cause the second natural frequency of the main structure and the frequency associated with the vibration absorber's near-zero amplitude to become closer or even match the absorber frequency. As indicated in Fig. 16. a, the second frequency is constant after a stiffness of 800 N/m. Therefore, this design dimension will satisfy the required measurement range of 0 to 800 N/m because saturation occurs after stiffness K_o = 800 N/m. Besides that, the absorber frequency value becomes closer to the second frequency, making the design suitable for this range.

Taking the force and displacement values of the results from the indentation test using MATLAB software to calculate the force-deformation ratio to get the exact force values at a deformation ratio of 10% for the four specimens A, B, C, and D respectively as indicated in Fig. 17. Using (15), Young's Modulus values for these specimens were calculated. Our findings revealed that these samples exhibited varying stiffness levels of stiffness are reported in Table II. Due to difference, Young's Modulus differed from the value of 10.12 to 226.89 kPa, resulting in observable shifts in their natural frequencies. The differences in stiffness among the PDMS samples directly contributed to the

observed frequency shifts as mentioned in the previous section of experimental measurements using the piezoelectric system.

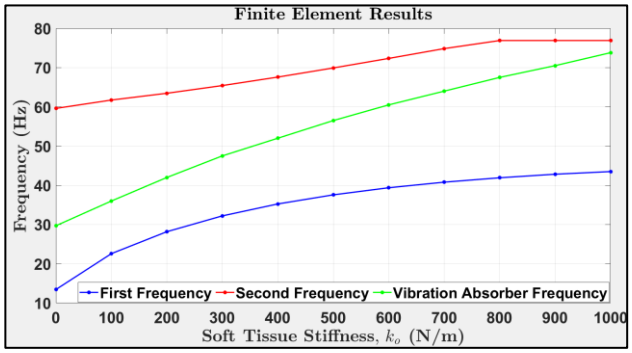

(a)

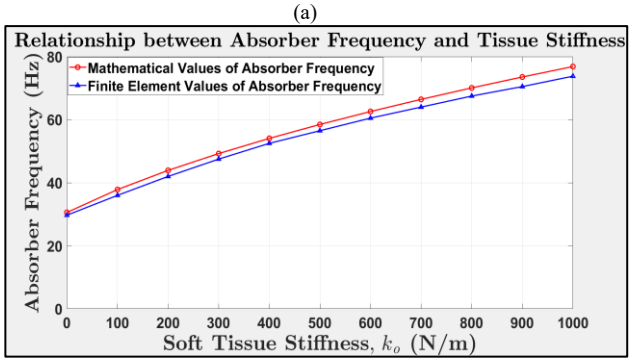

(b)

Fig. 16. (a) Finite element results for stiffness K_o range (0 – 1 kN/m), and (b) comparison between the mathematical results and finite element results of the vibration absorber

TABLE II. YOUNG'S MODULUS FOR DIFFERENT PDMS SPECIMENS MEASURED BY UNIVERSAL TESTING MACHINE

Specimen	PDMS mixing ratio (hardener to base)	Young's modulus (kPa)
Specimen A	1:50	10.12
Specimen B	1:40	22.53
Specimen C	1:30	82.75
Specimen D	1:20	226.89

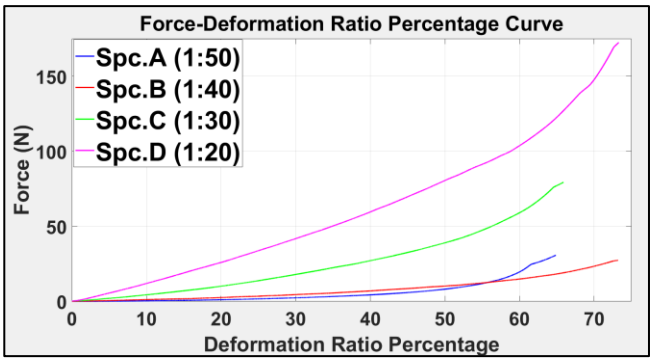

Fig. 17. Force-deformation ratio curve (a) A (1:50), (b) B (1:40), (c) C (1:30), and (d) D (1:20)

The change in the three frequencies is observed, and the mean readings based on five repetitions for each specimen ± 10 standard deviations of the repeatable measurements are reported in Fig. 18. Additionally, the system's frequency response (peak to peak) at no contact and specimens (A, B, C, D) in Fig. 19. The sensor's response was analyzed under different conditions: no contact (K_o = 0) and various stiffness levels using different PDMS specimens with different stiffness. Fluctuations in the stiffness of the tissue caused by the presence of diseased tissue led to alteration in the vibration absorber frequency, facilitating the subsequent detection of the diseased tissue as mentioned in [56], the stiffness of the liver's diseased tissue was discovered to be up to three times that of normal one.

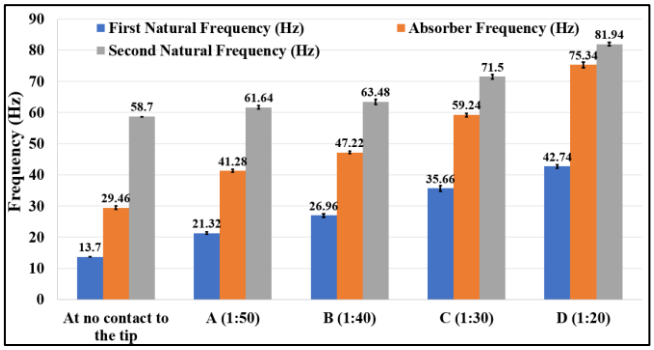

Fig. 18. The frequency change in the three frequencies for pdms specimens

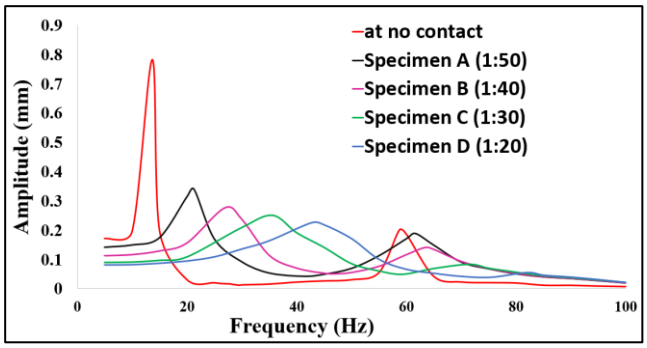

Fig. 19. Frequency response curve at no contact to the tip and specimens (A, B, C, D)

In this study, we experimentally tested four biological tissues (Gizzard, Breast, Heart, and Liver). The shift in three frequencies was recorded, and the frequency response curve for all specimens was plotted from the measured data, as shown in Fig. 20 and Fig. 21. Besides Their Young's modulus is estimated according to the previous measurements of PDMS specimens' curve as a reference in Fig. 22.

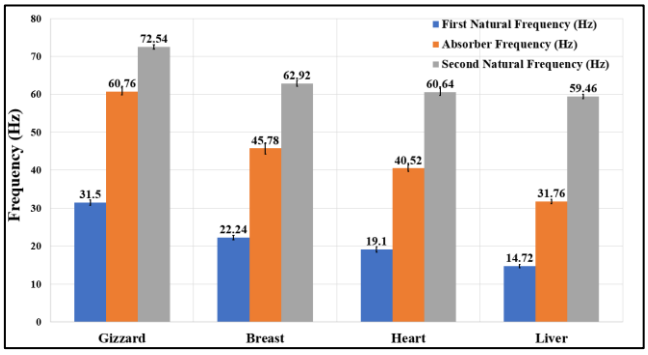

Fig. 20. The frequency change in the three frequencies for the gizzard, breast, heart, and liver

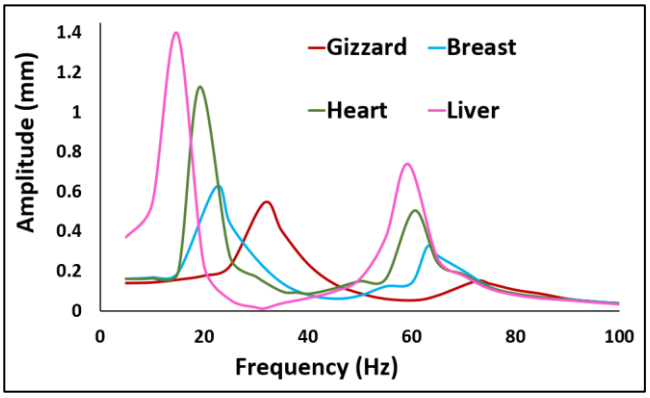

Fig. 21. Frequency response curve of the soft tissue samples

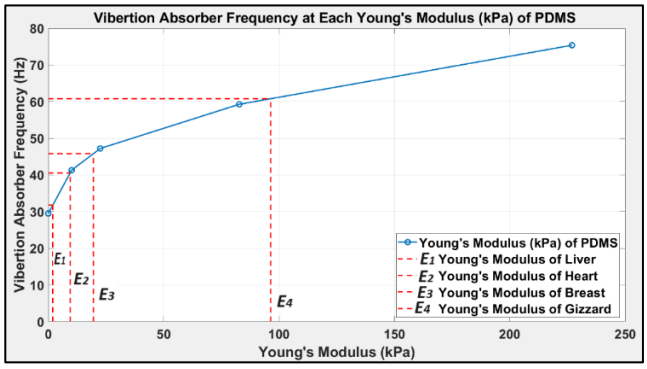

Fig. 22. Testing gizzard, breast, heart, and liver for estimating young's modulus

The Young's modulus (E) values for each tissue were reported in Table III ranging from 1.97 to 96.36 kPa.

TABLE III. YOUNG'S MODULUS VALUES OF SOFT TISSUE

Specimen	Young's Modulus (kPa)
Liver	1.97
Heart	9.47
Breast	19.55
Gizzard	96.36

IX. CONCLUSIONS

A detailed design methodology for the parameters of tactile sensors dedicated to compliance detection has been presented. The sensing approach relies on using the vibration absorber frequency to achieve a non-invasive measurement, eliminating the need to operate at resonance, which could potentially harm the system and tissue during compliance detection. The optimization of sensor parameters is conducted to achieve the maximum measurement range and linearity. A simplified mathematical model is introduced using MATLAB and verified through finite element analysis with ANSYS. Due to a theoretical comparison between the two sensors with stiffness of 61 N/m and 188 N/m, the higher stiffness sensor gives the higher range of measurements and the best linearity that achieves accurate and reliable measurements. Subsequently, increasing the stiffness will increase linearity and the range of measurements, ensuring precision and accuracy in measurements. We carefully selected sensor design parameters to ensure effective vibration absorption. These parameters were optimized to provide a wide measurement range and strong linearity. As a result, the measurements for the second actuator range from 0 to 800 N/m, with an excellent linearity of R^2 = 97%. We presented a novel contact stiffness sensor specifically for detecting diseased tissue. This sensor is designed based on the concept of a (2-DOF) vibration absorber system.

The sensor's measuring range is chosen to cover typical Young's modulus values of diseased tissues, going up to 1 MPa, with an indentor radius of 1 mm, resulting in a stiffness range of 4 kN/m. To validate our concept, we created an experimental prototype, which revealed that the first resonance has a high deflection amplitude, making it more prone to failure. In contrast, the second resonance has a lower deflection amplitude. The sensor has been proven to be highly capable, providing precise and dependable compliance measurements of soft tissues such as the liver, heart, breast, and gizzard. It can accurately measure tissues with varying Young's modulus values, ranging from 1.97 to 96.36 kPa, and PDMS samples with stiffness values between 10.12 and 226.89 kPa. The results demonstrate the successful non-invasive detection of tissue differences by the proposed sensor, offering high sensitivity and linearity without necessitating significant tissue deformation or penetration. This innovation holds promise for improving the precision of tactile awareness in MIS, thereby contributing to enhanced surgical outcomes.

The sensor's capabilities significantly enhance clinical outcomes in MIS by accurately measuring tissue compliance, enabling precise differentiation of pathological tissues like during tumor resections or organ surgeries. This minimizes tissue damage, reducing surgical trauma and complications. For instance, it provides real-time feedback on tissue stiffness variations, aiding precise tumor removal while preserving healthy tissue. Its ability to measure a wide range of Young's modulus values in delicate procedures ensures optimal tissue handling and reduces inadvertent damage, enhancing surgical precision and patient safety through tailored treatment strategies. Integrating this sensor into MIS practices promises to advance surgical techniques and optimize patient care by improving tissue characterization and procedural accuracy.

X. FUTURE WORK

Looking forward, our research will focus on refining sensor design to enhance sensitivity across a wide frequency range, which is crucial for tissue characterization. We plan to integrate advanced signal processing techniques and Artificial Intelligence (AI), particularly Machine Learning Algorithms (MLA), to further optimize detection capabilities. This integrated approach promises to advance surgical techniques by providing surgeons with enhanced real-time feedback, facilitating early tumor detection and precise localization, ultimately improving overall patient outcomes.

ACKNOWLEDGMENTS

The first author is supported by a scholarship from the Egyptian Ministry of Higher Education (MoHE), which is gratefully acknowledged. We extend our thanks to the Science and Technology Development Fund project (STDF-12417 and STDF- 46702), and Japan International Cooperation Agency (JICA) for letting us use some equipment from the Micro Fabrication Center of E-JUST for this research.

REFERENCES

[1] K. Chen *et al.*, "Robot-Assisted Minimally Invasive Breast Surgery: Recent Evidence with Comparative Clinical Outcomes," *Journal of Clinical Medicine*, vol. 11, no. 7, 2022, doi: 10.3390/jcm11071827.

[2] D. Vo, B. Jiang, T. D. Azad, N. R. Crawford, A. Bydon, and N. Theodore, "Robotic Spine Surgery: Current State in Minimally Invasive Surgery," *Global Spine J*, vol. 10, no. 2, pp. 34S-40S, Apr. 2020, doi: 10.1177/2192568219878131.

[3] E. L. Moss, G. Morgan, A. P. Martin, P. Sarhanis, and T. Ind, "Surgical trends, outcomes and disparities in minimal invasive surgery for patients with endometrial cancer in England: A retrospective cohort study," *BMJ Open*, vol. 10, no. 9, Sep. 2020, doi: 10.1136/bmjopen-2019-036222.

[4] S. Klompmaker *et al*., "Outcomes after minimally-invasive versus open pancreatoduodenectomy: A pan-European propensity score matched study," *Ann Surg*, vol. 271, no. 2, pp. 356–363, Feb. 2020, doi: 10.1097/SLA.0000000000002850.

[5] P. C. Van Der Sluis, D. Schizas, T. Liakakos, and R. Van Hillegersberg, "Minimally Invasive Esophagectomy," *Digestive Surgery*, vol. 37, no. 2, pp. 93–100, Mar. 01, 2020. doi: 10.1159/000497456.

[6] J. Klodmann *et al*., "An Introduction to Robotically Assisted Surgical Systems: Current Developments and Focus Areas of Research," *Current Robotics Reports*, vol. 2, no. 3, pp. 321–332, Sep. 2021, doi: 10.1007/s43154-021-00064-3.

[7] G. Dagnino and D. Kundrat, "Robot-assistive minimally invasive surgery: trends and future directions," *International Journal of Intelligent Robotics and Applications*, 2024, doi: 10.1007/s41315-024-00341-2.

[8] Y. Liu, R. Bao, J. Tao, J. Li, M. Dong, and C. Pan, "Recent progress in tactile sensors and their applications in intelligent systems," *Science Bulletin*, vol. 65, no. 1, pp. 70–88, Jan. 15, 2020, doi: 10.1016/j.scib.2019.10.021.

[9] J. Zhu, C. Zhou, and M. Zhang, "Recent progress in flexible tactile sensor systems: from design to application," *Soft Science*, vol. 1, no. 1, 2021. doi: 10.20517/ss.2021.02.

[10] K. Kim *et al*., "Tactile Avatar: Tactile Sensing System Mimicking Human Tactile Cognition," *Advanced Science*, vol. 8, no. 7, Apr. 2021, doi: 10.1002/advs.202002362.

[11] Y. Lee and J. H. Ahn, "Biomimetic Tactile Sensors Based on Nanomaterials," *ACS Nano*, vol. 14, no. 2, pp. 1220–1226, Feb. 2020, doi: 10.1021/acsnano.0c00363.

[12] S. Chun *et al*., "An artificial neural tactile sensing system," *Nat Electron*, vol. 4, no. 6, pp. 429–438, Jun. 2021, doi: 10.1038/s41928-021-00585-x.

[13] J. Seetohul, M. Shafiee, and K. Sirlantzis, "Augmented Reality (AR) for Surgical Robotic and Autonomous Systems: State of the Art, Challenges, and Solutions," *Sensors*, vol. 23, no. 13, 2023, doi: 10.3390/s23136202.

[14] S. H. Cho *et al*., "High-Resolution Tactile-Sensation Diagnostic Imaging System for Thyroid Cancer," *Sensors*, vol. 23, no. 7, Apr. 2023, doi: 10.3390/s23073451.

[15] S. Zhao, C. C. Nguyen, T. T. Hoang, T. N. Do, and H. P. Phan, "Transparent Pneumatic Tactile Sensors for Soft Biomedical Robotics," *Sensors*, vol. 23, no. 12, Jun. 2023, doi: 10.3390/s23125671.

[16] H. H. Ly, Y. Tanaka, and M. Fujiwara, "Tumor Depth and Size Perception Using a Pneumatic Tactile Display in Laparoscopic Surgery," *IEEE Access*, vol. 9, pp. 167795–167811, 2021, doi: 10.1109/ACCESS.2021.3135698.

[17] C. H. Won, J. H. Lee, and F. Saleheen, "Tactile Sensing Systems for Tumor Characterization: A Review," *IEEE Sensors Journal*, vol. 21, no. 11, pp. 12578–12588, 2021, doi: 10.1109/JSEN.2021.3078369.

[18] A. M. R. F. El Bab, K. Sugano, T. Tsuchiya, O. Tabata, M. E. H. Eltaib, and M. M. Sallam, "Micromachined tactile sensor for soft-tissue compliance detection," *Journal of Microelectromechanical Systems*, vol. 21, no. 3, pp. 635–645, 2012, doi: 10.1109/JMEMS.2012.2184080.

[19] A. M. R. Fath El Bab and K. I. E. Ahmed, "A novel tactile sensor design for stiffness detection of soft tissues," in *ASME International Mechanical Engineering Congress and Exposition, Proceedings (IMECE)*, pp. 439–446, 2010, doi: 10.1115/IMECE2010-38794.

[20] A. M. R. Fath El-Bab, M. E. H. Eltaib, M. M. Sallam, and O. Tabata, "Tactile Sensor for Compliance Detection," *Sensors and Materials*, vol. 19, no. 3, pp. 165–177, 2007.

[21] C. Chircov and A. M. Grumezescu, "Microelectromechanical Systems (MEMS) for Biomedical Applications," *Micromachines*, vol. 13, no. 2, 2022, doi: 10.3390/mi13020164.

[22] R. Hajare, V. Reddy, and R. Srikanth, "MEMS based sensors – A comprehensive review of commonly used fabrication techniques," in *Materials Today: Proceedings*, pp. 720–730, 2021, doi: 10.1016/j.matpr.2021.05.223.

[23] M. Shikida, Y. Hasegawa, M. S. Al Farisi, M. Matsushima, and T. Kawabe, "Advancements in MEMS technology for medical applications: Microneedles and miniaturized sensors," *Japanese Journal of Applied Physics*, vol. 61, 2022.

[24] H. Liu *et al*., "A Piezoresistive-based 3-axial MEMS Tactile Sensor and Its Integrated Surgical Forceps for Gastrointestinal Endoscopic Minimally Invasive Surgery," 2024, doi: 10.21203/rs.3.rs-4483564/v1.

[25] X. Li and H. Yang, "Enhanced Bulk Micromachining Based on MIS Process," *3D and Circuit Integration of MEMS*, pp. 49-59 2021.

[26] A. A. M. Faudzi, Y. Sabzehmeidani, and K. Suzumori, "Application of micro-electro-mechanical systems (MEMS) as sensors: A review," *Journal of Robotics and Mechatronics*, vol. 32, no. 2, pp. 281–288, 2020, doi: 10.20965/jrm.2020.p0281.

[27] U. H. Shah, R. Muthusamy, D. Gan, Y. Zweiri, and L. Seneviratne, "On the Design and Development of Vision-based Tactile Sensors," *Journal of Intelligent and Robotic Systems: Theory and Applications*, vol. 102, no. 4, Aug. 2021, doi: 10.1007/s10846-021-01431-0.

[28] P. Roberts, M. Zadan, and C. Majidi, "Soft Tactile Sensing Skins for Robotics," *Current Robotics Reports*, vol. 2, no. 3, pp. 343–354, Jul. 2021, doi: 10.1007/s43154-021-00065-2.

[29] J. Zhang, S. Lai, H. Yu, E. Wang, X. Wang, and Z. Zhu, "Fruit Classification Utilizing a Robotic Gripper with Integrated Sensors and Adaptive Grasping," *Math Probl Eng*, vol. 2021, 2021, doi: 10.1155/2021/7157763.

[30] J. Lin *et al*., "Non-destructive fruit firmness evaluation using a soft gripper and vision-based tactile sensing," *Comput Electron Agric*, vol. 214, Nov. 2023, doi: 10.1016/j.compag.2023.108256.

[31] C. T. Nnodim, A. M. R. Fath El-Bab, B. W. Ikua, and D. N. Sila, "Design, Simulation, and Experimental Testing of a Tactile Sensor for Fruit Ripeness Detection," in *Transactions on Engineering Technologies: World Congress on Engineering and Computer Science 2019*, pp. 59–73, 2021, doi: 10.1007/978-981-15-9209-6_5.

[32] G. Runel, N. Lopez-ramirez, J. Chlasta, and I. Masse, "Biomechanical properties of cancer cells," *Cells*, vol. 10, no. 4, 2021, doi: 10.3390/cells10040887.

[33] B. Deng, Z. Zhao, W. Kong, C. Han, X. Shen, and C. Zhou, "Biological role of matrix stiffness in tumor growth and treatment," *Journal of Translational Medicine*, vol. 20, no. 1, 2022.

[34] A. Barkovskaya, A. Buffone, M. Žídek, and V. M. Weaver, "Proteoglycans as Mediators of Cancer Tissue Mechanics," *Frontiers in Cell and Developmental Biology*, vol. 8, 2020.

[35] A. Micalet, E. Moeendarbary, and U. Cheema, "3D In Vitro Models for Investigating the Role of Stiffness in Cancer Invasion," *ACS Biomaterials Science and Engineering*, vol. 9, no. 7, pp. 3729–3741, Jul. 10, 2023, doi: 10.1021/acsbiomaterials.0c01530.

[36] M. K. Hayward, J. M. Muncie, and V. M. Weaver, "Tissue mechanics in stem cell fate, development, and cancer," *Developmental Cell*, vol. 56, no. 13, pp. 1833–1847, Jul. 12, 2021.

[37] H. T. Nia, L. L. Munn, and R. K. Jain, "Physical traits of cancer," *Science (1979)*, vol. 370, no. 6516, Oct. 2020, doi: 10.1126/SCIENCE.AAZ0868.

[38] S. Ishihara and H. Haga, "Matrix Stiffness Contributes to Cancer Progression by Regulating Transcription Factors," *Cancers*, vol. 14, no. 4, 2022, doi: 10.3390/cancers14041049.

[39] F. Sauer *et al*., "Changes in Tissue Fluidity Predict Tumor Aggressiveness In Vivo," *Advanced Science*, vol. 10, no. 26, Sep. 2023, doi: 10.1002/advs.202303523.

[40] A. Souhami *et al*., "Similar performance of liver stiffness measurement and liver surface nodularity for the detection of portal hypertension in patients with hepatocellular carcinoma," *JHEP Reports*, vol. 2, no. 5, Oct. 2020, doi: 10.1016/j.jhepr.2020.100147.

[41] J. Yoo *et al*., "Tumor stiffness measured by shear wave elastography correlates with tumor hypoxia as well as histologic biomarkers in breast cancer," *Cancer Imaging*, vol. 20, no. 1, Dec. 2020, doi: 10.1186/s40644-020-00362-7.

[42] L. Scimeca, P. Maiolino, E. Bray, and F. Iida, "Structuring of tactile sensory information for category formation in robotics palpation," *Auton Robots*, vol. 44, no. 8, pp. 1377–1393, Nov. 2020, doi: 10.1007/s10514-020-09931-y.

[43] Y. Yang, K. L. Yung, T. W. R. Hung, and K. M. Yu, "Analyzing Liver Surface Indentation for In Vivo Refinement of Tumor Location in Minimally Invasive Surgery," *Ann Biomed Eng*, vol. 49, no. 5, pp. 1402–1415, May 2021, doi: 10.1007/s10439-020-02698-4.

[44] A. Candito *et al*., "Identification of tumor nodule in soft tissue: An inverse finite-element framework based on mechanical characterization," *Int J Numer Method Biomed Eng*, vol. 36, no. 8, Aug. 2020, doi: 10.1002/cnm.3369.

[45] J. Palacio-Torralba, R. L. Reuben, and Y. Chen, "A novel palpation–based method for tumor nodule quantification in soft tissue—computational framework and experimental validation," *Med Biol Eng Comput*, vol. 58, no. 6, pp. 1369–1381, Jun. 2020, doi: 10.1007/s11517-020-02168-y.

[46] A. Tsitlakidis *et al*., "Atomic force microscope nanoindentation analysis of diffuse astrocytic tumor elasticity: Relation with tumor histopathology," *Cancers (Basel)*, vol. 13, no. 18, Sep. 2021, doi: 10.3390/cancers13184539.

[47] A. Saracino, T. J. C. Oude-Vrielink, A. Menciassi, E. Sinibaldi, and G. P. Mylonas, "Haptic Intracorporeal Palpation Using a Cable-Driven Parallel Robot: A User Study," *IEEE Trans Biomed Eng*, vol. 67, no. 12, pp. 3452–3463, Dec. 2020, doi: 10.1109/TBME.2020.2987646.

[48] M. O. Shaikh, C. M. Lin, D. H. Lee, W. F. Chiang, I. H. Chen, and C. H. Chuang, "Portable Pen-Like Device with Miniaturized Tactile Sensor for Quantitative Tissue Palpation in Oral Cancer Screening," *IEEE Sens J*, vol. 20, no. 17, pp. 9610–9617, Sep. 2020, doi: 10.1109/JSEN.2020.2992767.

[49] M. H. Lu and Y. P. Zheng, "Indentation test of soft tissues with curved substrates: A finite element study," *Medical & Biological Engineering & Computing*, vol. 42, no. 4, pp.535-540, 2004.

[50] B. Ahn and J. Kim, "Measurement and characterization of soft tissue behavior with surface deformation and force response under large deformations," *Med Image Anal*, vol. 14, no. 2, pp. 138–148, Apr. 2010, doi: 10.1016/j.media.2009.10.006.

[51] S. Kalyanam, K. S. Toohey, and M. F. Insana, "Modeling biphasic hydrogels under spherical indentation: Application to soft tissues," *Mechanics of Materials*, vol. 161, Oct. 2021, doi: 10.1016/j.mechmat.2021.103987.

[52] J. Zemła *et al*., "Indenting soft samples (hydrogels and cells) with cantilevers possessing various shapes of probing tip," *European Biophysics Journal*, vol. 49, no. 6, pp. 485–495, Sep. 2020, doi: 10.1007/s00249-020-01456-7.

[53] A. Fouly, M. N. A. Nasr, A. M. R. F. El Bab, and A. A. Abouelsoud, "Design, Modeling and Simulation of a Micro Tactile Sensor for Soft Tissue Stiffness Measurement with Three Tips Configuration," in *Proceedings of International Conference on Computational Intelligence, Modelling and Simulation*, pp. 155–160, 2016, doi: 10.1109/CIMSim.2015.28.

[54] D. Xu *et al*., "Measuring the elastic modulus of soft biomaterials using nanoindentation," journal of the mechanical behavior of biomedical materials, vol. 133, p. 105329 Sep. 2022, doi: 10.1016/j.jmbbm.2022.105329.

[55] C. F. Guimarães, L. Gasperini, A. P. Marques, and R. L. Reis, "The stiffness of living tissues and its implications for tissue engineering," *Nature Reviews Materials*, vol. 5, no. 5, pp. 351–370, May 01, 2020. doi: 10.1038/s41578-019-0169-1.

[56] F. J. Carter, T. G. Frank, P. J. Davies, D. Mclean, and A. Cuschieri, "Measurements and modelling of the compliance of human and porcine organs," *Medical Image Analysis*, vol. 5, no, 4, pp.231-236, 2001.

[57] A. Gefen and S. S. Margulies, "Are in vivo and in situ brain tissues mechanically similar?," *journal of biomechanics*, vol. 37, no. 9, pp. 1339–1352, Sep. 2004, doi: 10.1016/j.jbiomech.2003.12.032.

[58] Z. Taylor and K. Miller, "Reassessment of brain elasticity for analysis of biomechanisms of hydrocephalus," *journal of biomechanics*, vol. 37, no. 8, pp. 1263–1269, Aug. 2004, doi: 10.1016/j.jbiomech.2003.11.027.

[59] K. A. Athanasiou, M. P. Rosenwasser, J. A. Buckwalter, T. I. Malinin, and V. C. Mow, "Interspecies comparisons of in situ intrinsic mechanical properties of distal femoral cartilage," *Journal of orthopaedic Research*, vol. 9, no. 3, pp. 330–340, 1991, doi: 10.1002/jor.1100090304.

[60] U. Kim, Y. B. Kim, D. Y. Seok, J. So, and H. R. Choi, "A surgical palpation probe with 6-axis force/torque sensing capability for minimally invasive surgery," *IEEE Transactions on Industrial Electronics*, vol. 65, no. 3, pp. 2755–2765, Mar. 2018, doi: 10.1109/TIE.2017.2739681.

[61] J. Kim, B. K. Tay, N. Stylopoulos, D. W. Rattner, and M. A. Srinivasan, "Characterization of intra-abdominal tissues from in vivo animal experiments for surgical simulation," In *International Conference on Medical Image Computing and Computer-Assisted Intervention*, pp. 206-213. 2003, doi: 10.1007/978-3-540-39899-8_26.

[62] Y. Al-Handarish *et al*., "A Survey of Tactile-Sensing Systems and Their Applications in Biomedical Engineering," *Advances in Materials Science and Engineering*, vol. 2020, 2020, doi: 10.1155/2020/4047937.

[63] G. Ma and M. Soleimani, "Spectral Capacitively Coupled Electrical Resistivity Tomography for Breast Cancer Detection," *IEEE Access*, vol. 8, pp. 50900–50910, 2020, doi: 10.1109/ACCESS.2020.2980112.

[64] P. Sadeghi, K. Moran, and J. L. Robar, "Capacitive monitoring system for real-time respiratory motion monitoring during radiation therapy," *Journal of Applied Clinical Medical Physics*, vol. 21, no. 9, pp. 16–24, Sep. 2020, doi: 10.1002/acm2.12958.

[65] O. Semeniuk, P. Sadeghi, J. D. Farah, K. Moran, and J. Robar, "Performance optimization of capacitive motion sensing (CMS) system for intra-fraction motion detection during stereotactic radiosurgery," *Biomedical physics & engineering express*, vol. 6, no. 1, 2020, doi: 10.1088/2057-1976/ab5bff.

[66] G. Zonta, G. Rispoli, C. Malagù, and M. Astolfi, "Overview of Gas Sensors Focusing on Chemoresistive Ones for Cancer Detection," *Chemosensors*, vol. 11, no. 10, 2023, doi: 10.3390/chemosensors11100519.

[67] Y. Peng, N. Yang, Q. Xu, Y. Dai, and Z. Wang, "Recent advances in flexible tactile sensors for intelligent systems," *Sensors*, vol. 21, no. 16, 2021, doi: 10.3390/s21165392.

[68] M. Astolfi, G. Rispoli, G. Anania, G. Zonta, and C. Malagù, "Chemoresistive Nanosensors Employed to Detect Blood Tumor Markers in Patients Affected by Colorectal Cancer in a One-Year Follow Up," *Cancers (Basel)*, vol. 15, no. 6, Mar. 2023, doi: 10.3390/cancers15061797.

[69] R. Pan, K. Hu, R. Jia, S. A. Rotenberg, D. Jiang, and M. V Mirkin, "Resistive-Pulse Sensing Inside Single Living Cells," *Journal of the American Chemical Society*, vol. 142, no. 12, pp.5778-5784, 2020.

[70] S. Pohtongkam and J. Srinonchat, "Tactile object recognition for humanoid robots using new designed piezoresistive tactile sensor and dcnn," *Sensors*, vol. 21, no. 18, Sep. 2021, doi: 10.3390/s21186024.

[71] T. D. Nguyen and J. S. Lee, "Recent development of flexible tactile sensors and their applications," *Sensors*, vol. 22, no. 1, 2022, doi: 10.3390/s22010050.

[72] W. Yue *et al*., "Dynamic Piezoelectric Tactile Sensor for Tissue Hardness Measurement Using Symmetrical Flexure Hinges and Anisotropic Vibration Modes," *IEEE Sensor Journal*, vol. 21, no. 16, pp. 17712–17722, Aug. 2021, doi: 10.1109/JSEN.2021.3086114.

[73] O. A. Lindahl, T. Backlund, K. Ramser, P. Liv, B. Ljungberg, and A. Bergh, "A tactile resonance sensor for prostate cancer detection - Evaluation on human prostate tissue," *Biomedical Physics & Engineering Express*, vol. 7, no. 2, Mar. 2021, doi: 10.1088/2057-1976/abe681.

[74] W. Lin, B. Wang, G. Peng, Y. Shan, H. Hu, and Z. Yang, "Skin-Inspired Piezoelectric Tactile Sensor Array with Crosstalk-Free Row+Column Electrodes for Spatiotemporally Distinguishing Diverse Stimuli," *Advanced Science*, vol. 8, no. 3, Feb. 2021, doi: 10.1002/advs.202002817.

[75] C. Ge and E. Cretu, "A Polymeric Piezoelectric Tactile Sensor Fabricated by 3D Printing and Laser Micromachining for Hardness Differentiation during Palpation," *Micromachines*, vol. 13, no. 12, Dec. 2022, doi: 10.3390/mi13122164.

[76] V. T. Rathod, "A review of acoustic impedance matching techniques for piezoelectric sensors and transducers," *Sensors*, vol. 20, no. 14, pp. 1–65, 2020, doi: 10.3390/s20144051.

[77] K. Kim, J. Kim, X. Jiang, and T. Kim, "Static Force Measurement Using Piezoelectric Sensors," *Journal of Sensors*, vol. 2021, 2021, doi: 10.1155/2021/6664200.

[78] G. Wu, M. Gotthardt, and M. Gollasch, "Assessment of nanoindentation in stiffness measurement of soft biomaterials: kidney, liver, spleen and uterus," *Scientific reports*, vol. 10, no. 1, p.18784, Dec. 2020, doi: 10.1038/s41598-020-75738-7.

[79] C. Huang, Q. Wang, M. Zhao, C. Chen, S. Pan, and M. Yuan, "Tactile Perception Technologies and Their Applications in Minimally Invasive Surgery: A Review," *Frontiers in Physiology*, vol. 11, p.611596, Dec. 23, 2020, doi: 10.3389/fphys.2020.611596.

[80] A. Gutierrez-Giles, M. A. Padilla-Castañeda, L. Alvarez-Icaza, and E. Gutierrez-Herrera, "Force-Sensorless Identification and Classification of Tissue Biomechanical Parameters for Robot-Assisted Palpation," *Sensors*, vol. 22, no. 22, Nov. 2022, doi: 10.3390/s22228670.

[81] S. S. Kumat and P. S. Shiakolas, "Design, Prototyping, and Characterization of a Micro-Force Sensor Intended for Tissue Assessment in Confined Spaces," *IEEE Sensors Journal*., vol. 24, no. 12, p. 18937, 2024, doi: 10.1109/JSEN.2024.3395975.

[82] C. Wang *et al*., "Tissue-Adhesive Piezoelectric Soft Sensor for In Vivo Blood Pressure Monitoring During Surgical Operation," *Advanced Functional Materials*, vol. 33, no. 38, Sep. 2023.

[83] Y. Tang, S. Liu, Y. Deng, Y. Zhang, L. Yin, and W. Zheng, "An improved method for soft tissue modeling," *Biomed Signal Process Control*, vol. 65, Mar. 2021, doi: 10.1016/j.bspc.2020.102367.

[84] Z. Nie, J. W. Kwak, M. Han, and J. A. Rogers, "Mechanically Active Materials and Devices for Bio-Interfaced Pressure Sensors – A Review," *Advanced Materials*, p. 2205609, 2023, doi: 10.1002/adma.202205609.

[85] H. Xie, J. Song, Y. Zhong, and C. Gu, "Kalman Filter Finite Element Method for Real-Time Soft Tissue Modeling," *IEEE Access*, vol. 8, pp. 53471–53483, 2020, doi: 10.1109/ACCESS.2020.2981400.

[86] L. Gan, W. Duan, T. O. Akinyemi, W. Du, O. M. Omisore, and L. Wang, "Development of a Fiber Bragg Grating-Based Force Sensor for Minimally Invasive Surgery-Case Study of Ex-Vivo Tissue Palpation," *IEEE Transactions on Instrumentation and Measurement*, vol. 72, pp. 1-12, 2023, doi: 10.1109/TIM.2021.3136179.

[87] S. Chauhan and M. Z. Ansari, "Vacuum-assisted piezoelectric cantilever mass sensor performance," *Journal of Mechanical Science and Technology*, vol. 35, no. 12, pp. 5489–5494, Dec. 2021.

[88] S. Chauhan and M. Z. Ansari, "Frequency response of a self-actuating cantilever sensor immersed in fluid," *Journal of Mechanical Science and Technology*, vol. 35, no. 4, pp. 1457–1462, Apr. 2021.

[89] X. Gao *et al*., "Piezoelectric Actuators and Motors: Materials, Designs, and Applications," *Advanced Materials Technologies*, vol. 5, no. 1, 2020, doi: 10.1002/admt.201900716.

[90] S. Mohith, A. R. Upadhya, K. P. Navin, S. M. Kulkarni, and M. Rao, "Recent trends in piezoelectric actuators for precision motion and their applications: a review," *Smart Materials and Structures*, vol. 30, no. 1, 2021, doi: 10.1088/1361-665X/abc6b9.

[91] K. Kapat, Q. T. H. Shubhra, M. Zhou, and S. Leeuwenburgh, "Piezoelectric Nano-Biomaterials for Biomedicine and Tissue Regeneration," *Advanced Functional Materials*, vol. 30, no. 44, 2020.

[92] P. Poillot, C. L. Le Maitre, and J. M. Huyghe, "The strain-generated electrical potential in cartilaginous tissues: a role for piezoelectricity," *Biophysical Reviews*, vol. 13, no. 1, pp. 91-100, 2021.

[93] A. Carter, K. Popowski, K. Cheng, A. Greenbaum, F. S. Ligler, and A. Moatti, "Enhancement of Bone Regeneration through the Converse Piezoelectric Effect, A Novel Approach for Applying Mechanical Stimulation," *Bioelectricity*, vol. 3, no. 4, pp. 255–271, 2021.

[94] Y. Zhang, F. Ju, X. Wei, D. Wang, and Y. Wang, "A piezoelectric tactile sensor for tissue stiffness detection with arbitrary contact angle," *Sensors*, vol. 20, no. 22, pp. 1–14, Nov. 2020, doi: 10.3390/s20226607.

[95] D. O. Uribe, J. Schoukens, and R. Stroop, "Improved Tactile Resonance Sensor for Robotic Assisted Surgery," *Mechanical Systems and Signal Processing*, vol. 99, pp. 600-610, 2018, doi: 10.1016/j.ymssp.2017.07.007.

[96] T. Sühn *et al*., "Vibro-acoustic sensing of tissue-instrument-interactions allows a differentiation of biological tissue in computerised palpation," Computers in Biology and Medicine, vol. 164, p.107272, Sep. 2023, doi: 10.1016/j.compbiomed.2023.107272.

[97] A. Esmaeel, K. I. E. Ahmed, and A. M. R. FathEl-Bab, "Determination of damping coefficient of soft tissues using piezoelectric transducer," Biomedical Microdevices, vol. 23, no. 2, Jun. 2021, doi: 10.1007/s10544-021-00558-z.

[98] Y. Yun *et al*., "A resonant tactile stiffness sensor for lump localization in robot-assisted minimally invasive surgery," *Proc Inst Mech Eng H*, vol. 233, no. 9, pp. 909–920, Sep. 2019, doi: 10.1177/0954411919856519.

[99] W. T. Thomson, *Theory of Vibration with Applications*. Springer US, 1993, doi: 10.1007/978-1-4899-6872-2.

[100] H. F. M. Ali, A. M. R. Fath El-Bab, Z. Zyada, and S. M. Megahed, "Novel Contact Sensor Concept and Prototype Based on 2-DOF Vibration Absorber System," in *Proceedings - International Conference on Intelligent Systems, Modelling and Simulation, ISMS*, pp. 89–94, Jul. 2016, doi: 10.1109/ISMS.2016.70.

[101] W. C. Hayes, L. M. Keer, G. Herrmann, and L. F. Mockros, "A mathematical analysis for indentation tests of articular cartilage," *Journal of biomechanics*, vol. 5, no. 5, pp. 541-551, 1972.

[102] A. M. R. F. El *et al*., "Design and Simulation of a Tactile Sensor for Soft-Tissue Compliance Detection Design and Simulation of a Tactile Sensor for Soft-Tissue Compliance Detection," *IEEJ Transactions on Sensors and Micromachines*, vol. 128, no. 5, pp. 186-192, 2008, doi: 10.1541/ieejsmas.128.186.

[103] M. Zhang, Y. P. Zheng, and A. F. T. Mak, "Estimating the effective Young's modulus of soft tissues from indentation tests-nonlinear finite element analysis of effects of friction and large deformation," *Medical engineering & physics*, vol. 19, no. 6, pp. 512-517, 1997, doi: 10.1016/S1350-4533(97)00017-9.

[104] W. F. Stokey. *vibration of systems having distributed mass and elasticity*. Shock and vibration handbook, pp. 7-14, 2002.

[105] L. Zhang, F. Ju, Y. Cao, Y. Wang, and B. Chen, "A tactile sensor for measuring hardness of soft tissue with applications to minimally invasive surgery," *Sensors and Actuators A: Physical*, vol. 266, pp. 197–204, Oct. 2017, doi: 10.1016/j.sna.2017.09.012.

[106] C. H. Chuang, T. H. Li, I. C. Chou, and Y. J. Teng, "Piezoelectric tactile sensor for submucosal tumor detection in endoscopy," *Sensors and Actuators A: Physical*, vol. 244, pp. 299–309, Jun. 2016, doi: 10.1016/j.sna.2016.04.020.

[107] M. Vatankhah-Varnosfaderani *et al*., "Mimicking biological stress–strain behaviour with synthetic elastomers," *Nature*, vol. 549, no. 7673, pp. 497–501, Sep. 2017, doi: 10.1038/nature23673.

[108] Z. Wang. *Polydimethylsiloxane mechanical properties measured by macroscopic compression and nanoindentation techniques*. M.S. thesis, University of South Florida, 2011.

[109] D. Corning, "Information about dow Corning brand silicone encapsulants," *Dow Corning Electronics Division, Midland, MI*, 2003.

[110] A. P. C. Choi and Y. P. Zheng, "Estimation of Young's modulus and Poisson's ratio of soft tissue from indentation using two different-sized indentors: finite element analysis of the finite deformation effect," *Medical and Biological Engineering and Computing*, vol. 43, pp. 258-264, 2008, doi: 10.1007/BF02345964.

[111] A. Müller, M. C. Wapler, and U. Wallrabe, "A quick and accurate method to determine the Poisson's ratio and the coefficient of thermal expansion of PDMS," *Soft Matter*, vol. 15, no. 4, pp. 779–784, 2019, doi: 10.1039/c8sm02105h.